Laser and Particle Beams (2008), *26*, 425–432. Printed in the USA.

doi:10.1017/S0263034608000438

Measurement of charged particles and cavitation bubble expansion velocities in laser induced breakdown in water

A. NATH AND A. KHARE
Department of Physics, Indian Institute of Technology Guwahati, Assam, India
(RECEIVED 8 February 2008; ACCEPTED 2 June 2008)

Abstract

The measurement of charged particles and cavitation bubble expansion velocity is reported in a laser induced breakdown in water using beam deflection set-up. Effect of laser power on charged particles, cavitation bubble velocities and higher order bubble oscillations is also studied.

Keywords: Cavitation bubbles; Higher order bubble oscillations; Laser induced breakdown in water

1. INTRODUCTION

Laser induced ablation and breakdown in general and especially in liquids has been receiving much attention because of numerous applications. Pulsed laser induced ablation has been studied extensively for deposition of the thin films (Bashir *et al.*, 2007; Ozaki *et al.*, 2007; Weiger *et al.*, 2006; Veiko *et al.*, 2006; Wolowski *et al.*, 2007). There are few reports aimed at laser assisted micro-machining processes such as photo ablation, chemical etching, and surface cleaning (Ramanathan & Molian, 2001), where the material surface processes were performed under water, as it helps in cooling of heat affected zone and prevents redeposition of ablated materials. Recently pulsed laser ablation of a bulk target and also suspended powder (Lee *et al.*, 2006) inside a liquid medium is used to synthesize noble metal, semiconductor and metal oxide nanostructure (Mafune *et al.*, 2000; Chen *et al.*, 2007; Thareja & Shukla, 2007) materials in a controlled and size-selected manner. The nanoparticle has a unique size dependent magnetic, optical, and electrical property, which makes it a suitable candidate in the field of material science. Pulsed laser deposition has also been performed in liquids to prepare highly effective noble metal surface-enhanced raman scattering (SERS) substrates (Cui *et al.*, 2006). In the field of medical sciences, the laser induced breakdown process has been used for dissection or inactivation of cellular organelles, cytoskeletal filaments, and chromosomes with high spatial precision, noninvasive intraocular surgery mainly posterior capsulotom, which is frequently being done after cataract surgery, laser induced lithotripsy, angioplasty etc. (Venugopalan *et al.*, 2002; Vogel *et al.*, 1990, 1996). Most of the research work in the field of laser surgery is carried out by taking water as a model because the biological tissues and fluids contain 80–85% of water.

Laser-matter interaction especially in liquids is poorly understood. The phenomena have a highly complex, non-equilibrium, and transient character. In view of the above mentioned importance of laser processing in liquids, a great deal of research is required to understand the complete hydrodynamics of the process.

When a high power laser is focused inside a liquid media, optical breakdown takes place due to rapid vaporization and ionization of the media, mainly by focal heating. Once focal heating generates the starting free electrons and ions, avalanche ionization *via* inverse bremsstrahlung absorption leads to plasma formation (Puliafito & Steinert, 1984; Vogel *et al.*, 1996). On a larger time scale, plasma in liquids is replaced by vapor bubbles, which expand due to inertia of vaporized fluid mass to reach a state when inside pressure becomes less than the surrounding liquid. The bubble collapses under the static ambient pressure of the outside liquid. This sudden collapse of bubbles constitutes a phenomenon of cavitation which results in a release of large amount of energy. The pressure and temperature inside the bubble rises again and the bubble rebounds. The process continues until all its energy is dissipated into the

Address correspondence and reprint requests to: Alika Khare, Department of Physics, Indian Institute of Technology Guwahati, Guwahati-781039, Assam, India. E-mail: alika@iitg.ernet.in

surrounding liquid (Hickling & Plesset, 1964). The cavitation effect is the main driving source of laser assisted tissue cutting in a liquid media. Cavitation erosions helps in fragmentation of kidney stones, removal of thrombus in obstructed arteries etc (Palanker *et al.*, 1997; Shangguan *et al.*, 1997). The dynamics of cavitations bubble finds direct implementation in the double pulse laser induced breakdown spectroscopy (DP-LIBS) (Rai *et al.*, 2003). Here the first pulse produces the cavitation bubbles in water followed by excitation of plasma by the probe pulse inside the bubble resulting into relatively intense and narrow spectral emission due to gaseous state inside the bubble. This improves the sensitivity of LIBS technique underwater and hence has the potential for detection of trace elements in water, monitoring sensor for liquids, an analytical chemistry technique for analysis of sediments, rocks under ocean, monitoring corrosion extent in nuclear power plants and even clear identification of tissues, bones, different microbiological bacteria, carious teeth (Fang & Ahmad, 2007; Schade *et al.*, 2006; Michel *et al.*, 2006; Diedrich *et al.*, 2007; Samek *et al.*, 2001).

In this paper, we report variation in charge-particle and cavitation bubble velocity as a function of distance from the focal point in laser assisted plasma using beam deflection set-up.

2. EXPERIMENTAL SET-UP

The schematic of the experimental set-up is shown in Figure 1. A stainless steel double cross of internal diameter 50 mm is used as a liquid cell. Photograph of the liquid cell is shown in Figure 2. The top and bottom ports were terminated with blank flanges and all other ports were terminated with glass windows as shown in Figure 2. The second harmonic of Q-switched Nd: YAG laser (HYL-101) was focused with 15 cm lens into the liquid cell filled with de-ionized distilled water (conductivity $< 1\ \mu\Omega^{-1}$). This resulted in evaporation and ionization of water in the focal region which led to the formation of high density plasma. Beam deflection set-up, (Alti & Khare 2006*a*, 2006*b*) shown in Figure 1, was used to measure cavitation bubble and charge-particle velocity. The formation of plasma followed by cavitation bubbles resulted in change in refractive index, which in turn deflected the He-Ne beam. The deflected signal is captured by a photodiode (D1) and displayed *via* 50 Ω terminator on to the DSO (Tektronix TDS 2012)

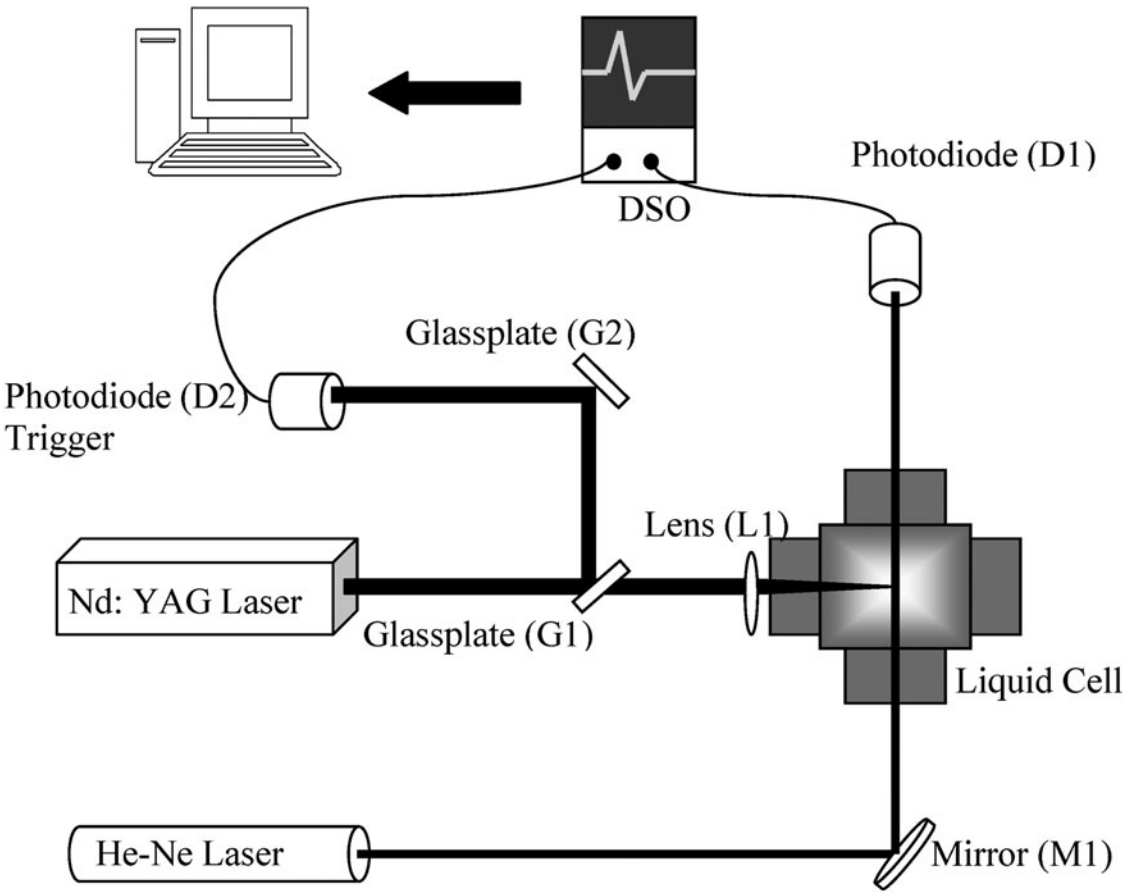

Fig. 1. Schematic of experimental set-up.

https://doi.org/10.1017/S0263034608000438 Published online by Cambridge University Press

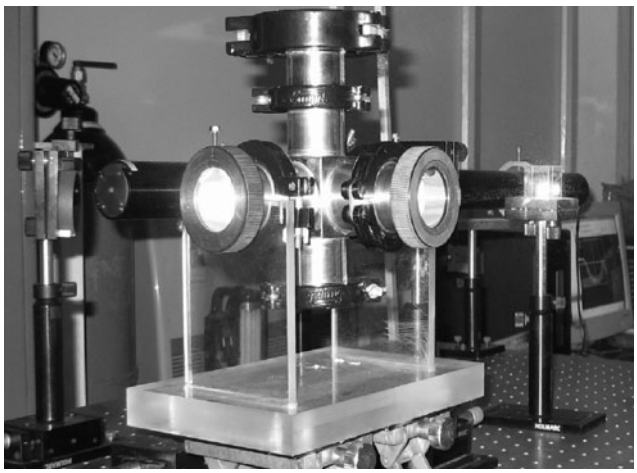

Fig. 2. Photograph of liquid cell.

interfaced with computer. The deflection is registered in the form of a dip (modulation) in the dc signal of a cw He-Ne laser. As the plasma plume is over, the He-Ne beam comes back to its original path and the photodiode output to its initial dc level. By measuring the relative delay of the deflected signal at the different positions, the velocities were estimated. The DSO was triggered by 4% of 4% reflection of Nd: YAG laser beam from microscopic glass plates G1 and G2, detected by photodiode D2.

3. RESULTS AND DISCUSSION

The complete oscilloscope trace of beam deflection signal is shown in Figure 3. Possible candidates for first negative narrow peak (inset a) could be high energetic electrons, and other charged particles. Focal heating by focusing high power laser inside the liquid cell generates the starting free electrons. The electron accelerates in the photon field of the source laser. The accelerated electron in turn ionizes other molecules and atoms. The process continues to generate ions and electrons resulting in plasma formation within the duration of laser pulse. On a larger time scale, recombination takes place and the plasma is replaced by cavitation bubbles whose main content is probably water vapor, hydrogen, and oxygen gas (Barnes & Rieckhoff, 1968). Cavitation bubbles undergo three stages; primary bubble collapse, rebound and higher order bubble formation. The second broad dip (Fig. 3.) at 170 mJ followed by third and fourth dip is attributed to first, second, and third order cavitation bubble oscillations, respectively. The inertia of vaporized fluid mass inside cavitation bubbles expands until all of its

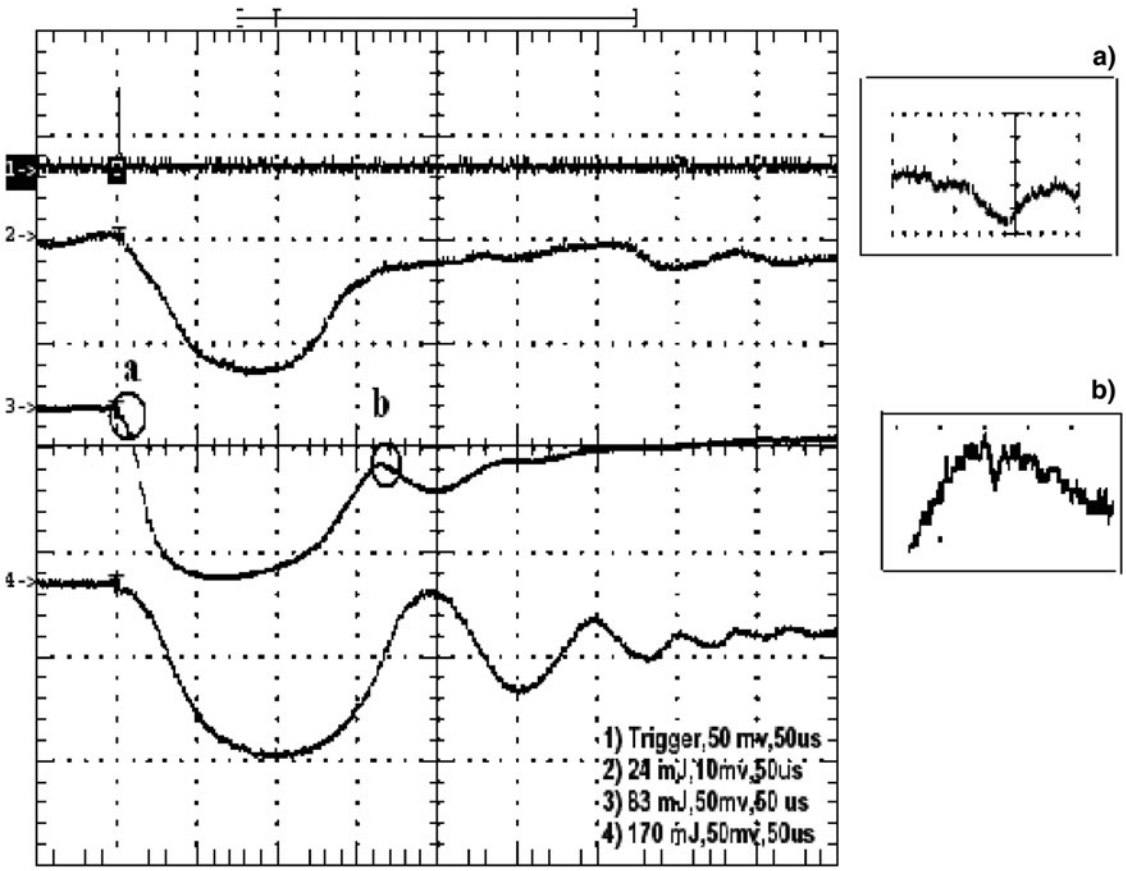

Fig. 3. Complete oscilloscope trace of deflected He-Ne signal at −1 mm from the focal region at different laser energies. (**a**) Charged-particles (**b**) Shockwaves.

https://doi.org/10.1017/S0263034608000438 Published online by Cambridge University Press

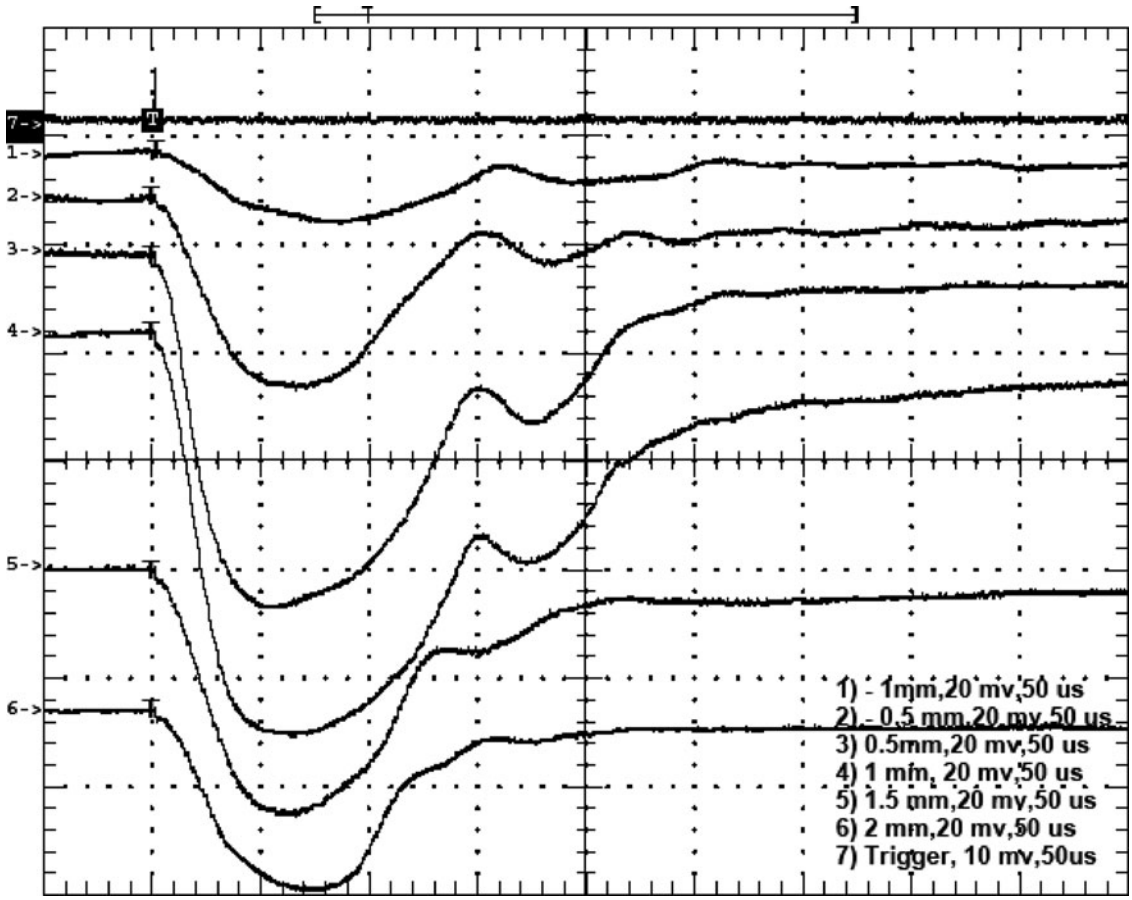

Fig. 4. Beam deflection traces of cavitation bubbles at 24 mJ. The 0 mm position corresponds to the focus.

kinetic energy is converted to potential energy to reach a state where the inside pressure becomes less than the hydrostatic pressure of the surrounding liquid. So the bubble collapses and the pressure inside it rises again. The process repeats and the bubble oscillates until all of its energy is dissipated into the surrounding liquid. Each time the bubble collapses, a shockwave is emitted which carries away the energy to the surrounding liquid. The emitted shockwave is shown on an expanded scale for 83 mJ laser pulse energy in inset of Figure 3b.

Figures 4 and 5 shows beam deflection signals at different positions both in forward and backward direction with respect to the focus of the high power laser for cavitations bubble and charged particles, respectively. The duration of charged particles is on the order of 1 μs. Therefore the signals were recorded separately at expanded scale of 1 μs/div, shown in Figure 5.

The variation of charged particles velocity with distance is shown in Figure 6. Near the focus, the velocity is in the range of 10^4 m/s. At a region away from the focus electrons are lost due to recombination, diffusion, and heat conduction. This results in cooling of plasma and a fluid dynamical process overtakes ionization reducing the velocities in the acoustic range. The variation of primary and secondary bubble velocities as a function of distance from the focus at different laser energies are shown in Figure 7. The trend observed is similar to that of the charged-particles, except that the velocities in this case are in subsonic range. As the energy carried away by the bubbles are smaller compared to the charged particles and so its appearance is confined to a smaller extent. The charged particles and cavitation bubbles velocity for different values of laser energies is listed in Table 1. It was observed that the backward velocity decays faster than the forward velocities because recoil momentum is more in the forward direction. As the laser-generated bubbles are not in equilibrium with the surrounding liquid so the bubble dissipates all of its energy by undergoing large numbers of oscillations. With each oscillation the bubble attenuates by emitting vaporized material and a shock wave in to the surrounding liquids. Subsequently higher order bubble velocities decrease.

The charged-particle velocity and cavitation bubbles velocity increases with increase in laser power. Higher order cavitation bubble oscillations becomes more pronounced with higher energy, as third, fourth, and even fifth order bubble oscillations in the subsonic range was observed at 170 mJ. This is because with the increase in laser energy the pressure gradient rises and the bubble becomes highly unstable. The oscillation of bubbles continues in order to balance the pressure difference which becomes more rigorous in case of higher energies.

https://doi.org/10.1017/S0263034608000438 Published online by Cambridge University Press

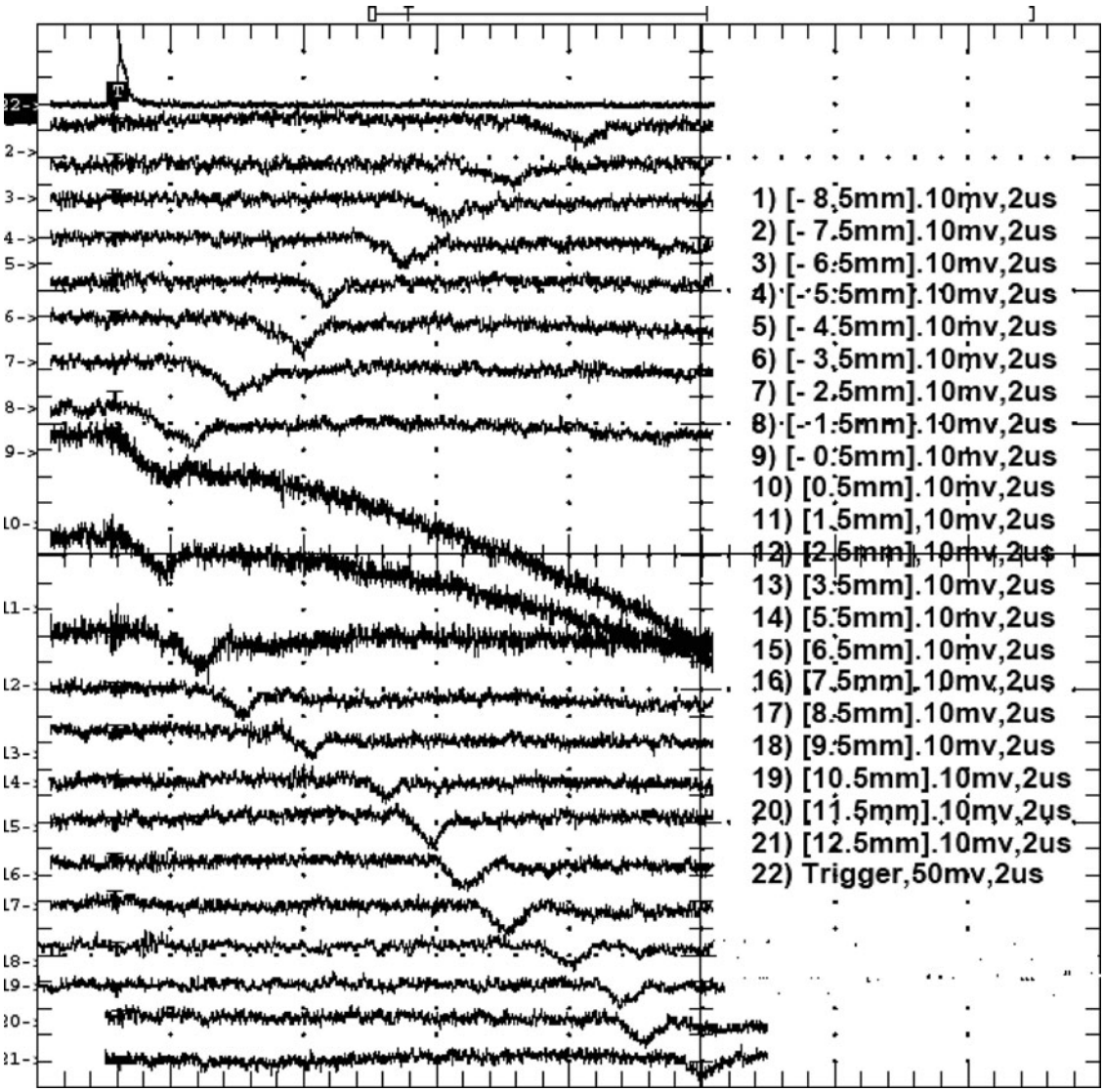

Fig. 5. Beam deflection traces of charged particles at different distances w.r.t the focus at 24 mJ. The 0 mm position corresponds to the focus.

We used Gilmore's model (Gilmore, 1952) to fit our experimental results of cavitation bubble velocity fields, throughout the liquid for different laser energies. It is assumed that no shock waves are emitted during the generation and collapse of the primary bubbles, so system is continuous and no jump conditions are required for conservation of momentum and conservation of mass equations given below:

$$\frac{\partial}{\partial t}(-\nabla\phi) + (\overline{u}\cdot\nabla)\overline{u} = -\frac{\nabla p}{\rho} + \frac{4\mu}{3\rho}\nabla(\nabla\cdot\overline{u}), \tag{1}$$

$$\overline{u} = -\nabla\phi, \tag{2}$$

$$\nabla\cdot\overline{u} = -\frac{1}{\rho}\left(\frac{\partial\rho}{\partial t} + u\frac{\partial\rho}{\partial r}\right). \tag{3}$$

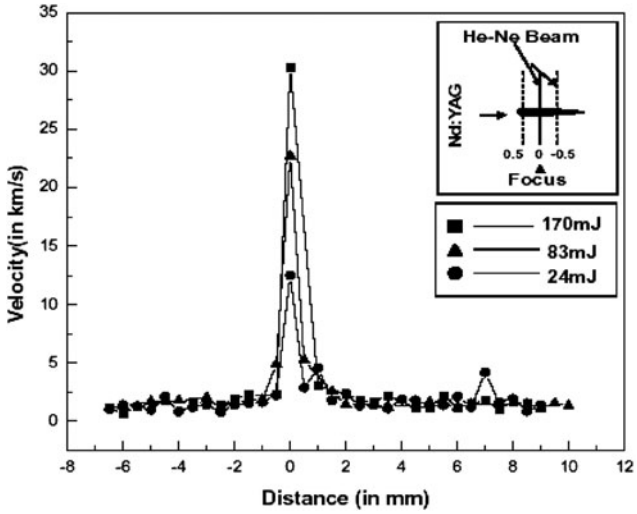

Fig. 6. Variation of velocity with distance for charged-particles.

https://doi.org/10.1017/S0263034608000438 Published online by Cambridge University Press

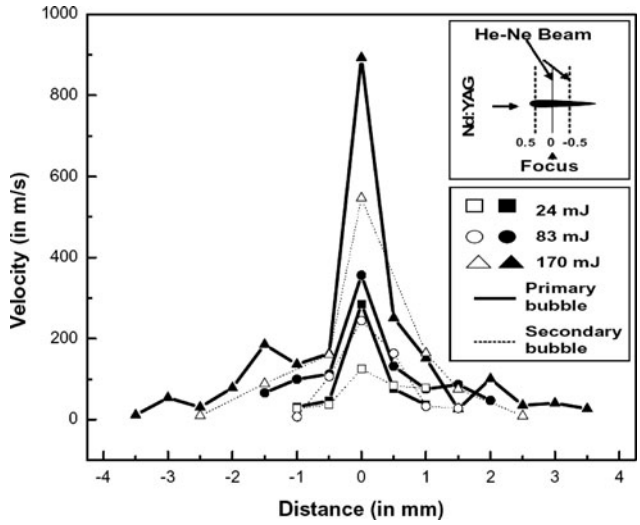

Fig. 7. Variation of velocity with distance for cavitation bubbles.

Where u is the vector velocity, ϕ is the velocity potential, p is the pressure, ρ is the density, μ is the viscosity of the liquid. Also the flow field in liquid can be described by the expression of spherical sound waves provided all velocities are small compared to sonic velocity in liquid, C_∞.

$$\phi = \frac{1}{r} f\left(t - \frac{r}{c_\infty}\right) \tag{4}$$

Under a spherically symmetric condition and by considering the above equations we arrive at the expression which describes the dynamics of cavitations bubble motion.

$$RU\frac{dU}{dR}\left(1 - \frac{U}{C}\right) + \frac{3}{2}U^2\left(1 - \frac{U}{3C}\right) = H\left(1 + \frac{U}{C}\right) + \frac{RU}{C}\frac{dH}{dR}\left(1 - \frac{U}{C}\right) \tag{5}$$

where R, C, H, U corresponds to the same parameters r, c, h, u (initially at liquids) at the bubble wall and h is the enthalpy difference. It was observed that the bubble wall velocity U varies as $R^{-1/2}$ when solved analytically. In order to derive the relations of velocity fields throughout the liquid (under quasi-acoustic approximation), the radial velocity is found by combining Eqs. (2) and (4).

$$u = \frac{f\left(t - \frac{r}{c_\infty}\right)}{r^2} + \frac{f'\left(t - \frac{r}{c_\infty}\right)}{{}^{r}c_\infty} \tag{6}$$

Eq. (6) is solved in an explicit analytical way to get the equation of velocity fields throughout the liquid:

$$u = U\left[\frac{R^2}{r^2} + \left(\frac{r^2 - R^2}{r^2}\right) \times \left(\frac{U^2}{2{c_\infty}^2} - \frac{P - p_\infty}{\rho {c_\infty}^2} - \frac{R}{2\rho {c_\infty}^2}\frac{dP}{dR}\right)\right] \tag{7}$$

The velocity field derived above is strictly confined to the subsonic range and hence fits to present experimental results of the primary bubbles velocity. In order to estimate the size of the bubble, we used Rayleigh's model (Rayleigh, 1917) of cavitation bubble.

$$R_{\max} = \frac{1}{0.915}\left(\frac{p - p_v}{\rho}\right)^{1/2} T_c \tag{8}$$

($R_{\max}$ is maximum bubble radius, p_v is the vapor pressure of water). The collapse time T_c equals half of the duration of the time interval between generation and first collapse of the bubble. Using Eqs. (7) and (8) theoretical values were estimated for the velocity fields. Since the contribution due to the first term in (7) is dominant, rest of the terms were neglected. Figure 8 compares the plots of primary bubbles velocities from the Gilmore's model discussed above and that of the obtained from beam deflection set-up for different laser energies. The theoretical model almost approximates the experimental points but at the focus it breaks down as it has an asymptotic nature with $1/r^2$ dependence. The experimental result shows some deviation with the theoretical model in the focal region, which may be attributed to multiple breakdowns as intensities are very high near the focus of the laser beam. However Gilmore model fits well at distances away from the focus.

Table 1. *Measured peak values of charged particles and cavitation bubble velocities and bubbles confinement distance*

Energy (mJ)	Charged-particle velocity (m/s)	Primary bubble velocity (m/s)	Secondary bubble velocity (m/s)	Third order bubble velocity (m/s)	Fourth order bubble velocity (m/s)	Fifth order bubble velocity (m/s)	Primary bubble confinement (mm)	Secondary bubble confinement (mm)
170	30×10^3	892	546	90	30	10	7	5
83	22×10^3	356	244	–	–	–	3.5	2.5
24	12×10^3	285	124	–	–	–	2	2

https://doi.org/10.1017/S0263034608000438 Published online by Cambridge University Press

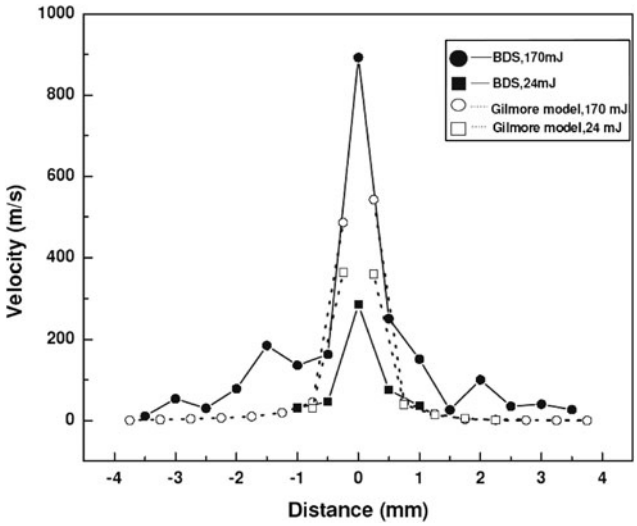

Fig. 8. Comparison of experimental and theoretical results.

4. CONCLUSION

The charged-particles and cavitation bubble velocities as a function of distance were measured for high power laser induced breakdown in distilled water. Beam deflection set-up was employed to measure the velocities. The velocity of charged particles and cavitation bubble increases with increase in laser energy. The charged particle velocities are of the order of 10^4 m/s whereas the primary and secondary bubbles velocities are in the acoustic region of few 100 m/s near the focal region. The higher order bubbles further slows down due to loss of energy into the surroundings. Cavitation bubbles oscillations are more pronounced at high laser power. We have used Rayleigh's model and Gilmore's model to fit experimental plots of primary bubbles velocity for different laser energies. Experimental and theoretical results show agreement at regions away from the focus.

REFERENCES

Alti, K. & Khare, A. (2006*a*). Low-energy low-divergence pulsed indium atomic beam by laser ablation. *Laser Part. Beams* **24**, 47–53.

Alti, K. & Khare, A. (2006*b*). Sculpted pulsed indium atomic beams via selective laser ablation of thin film. *Laser Part. Beams* **24**, 469–473.

Barnes, P. A. & Rieckhoff, K.E. (1968). Laser induced underwater sparks. *Appl. Phys. Lett*. **13**, 282–284.

Bashir, S., Rafique, M.S. & Ul-Haq, F. (2007). Laser ablation of ion irradiated CR-39. *Laser Part. Beams* **25**, 181–191.

Chen, X.Y., Cui, H., Liu, P. & Yang, G.W. (2007). Shape-induced ultraviolet absorption of CuO shuttlelike nanoparticles. *Appl. Phys. Lett*. **90**, 1831181–1831183.

Cui, H., Liu, P. & Yang, G.W. (2006). Noble metal nanoparticle patterning deposition using pulsed-laser deposition in liquid for surface-enhanced Raman scattering. *Appl. Phys. Lett*. **89**, 1531241–1531243.

Diedrich, J., Rehse, S.J. & Palchaudhuri, S. (2007). *Escherichia coli* identification and strain discrimination using nanosecond laser-induced breakdown spectroscopy, *Appl. Phys. Lett*. **90**, 1639011–1639011.

Fang, X. & Ahmad, S.R. (2007). Saturation effect at high laser pulse energies in laser-induced breakdown spectroscopy for elemental analysis in water. *Laser Part. Beams* **25**, 613–620.

Gilmore, F.R. (1952). The growth or collapse of a spherical bubble in a viscous compressible liquid. *CA. Inst. Techn. Repub*. **26**, 4.

Hickling, R. & Plesset, M.S. (1964). Collapse and rebound of a spherical bubble in water. *Phys. Fluids* **7**, 7–14.

Lee, J., Kim, D. & Kang, W. (2006). Preparation of Cu nanoparticles from Cu powder dispersed in 2-propanol by laser ablation. *Bull. Korean Chem. Soc*. **27**, 1869–1872.

Mafune, F., Kohno, J., Takeda, Y., Kondow, T. & Sawabe, H. (2000). Formation and size control of silver nanoparticles by laser ablation in aqueous solution. *J. Phys. Chem. B* **104**, 9111–9117.

Michel, A.P.M., Farr, N.E. & Chave, A.D. (2006). Evaluation of laser-induced breakdown spectroscopy(LIBS) as a new *in situ* chemical sensing technique for the deep ocean, *Proc. IEEE, Oceans 2006*, 1–5.

Ozaki, T., Bom, L.B.E., Ganeev, R., Kieffer, J.C., Suzuki, M. & Kuroda, H. (2007). Intense harmonic generation from silver ablation. *Laser Part. Beams* **25**, 321–325.

Palanker, D., Turovets, I. & Lewis, A. (1997). Dynamics of ArF excimer laser-induced cavitation bubbles in gel surrounded by a liquid medium. *Lasers Surgery & Medicine* **21**, 294–300.

Puliafito, C.A. & Steinert, R.F. (1984). Short-pulsed Nd:YAG laser microsurgery of the eye:biophysical consideration. *IEEE J.QE* **20**, 1442–1448.

Rai, V.N., Yueh, F. & Singh, J.P. (2003). Study of laser-induced breakdown emission from liquid under double-pulse excitation. *App. Opt*. **42**, 2094–2101.

Ramanathan, D. & Molian, P.A. (2001). Laser micromachinig using liquid optics. *Appl. Phys. Lett*. **78**, 1484–1486.

Rayleigh, L. (1917). On the pressure developed in a liquid during the collapse of a spherical cavity. *Phil. Magazine* **34**, 94–98.

Samek, O., Telle, H.H. & Beddows, D.C.S. (2001). Laser-induced breakdown spectroscopy: A tool for real-time, *in vitro* and *in vivo* identification of carious teeth. *BMC Oral Health* **1**, 1–9.

Schade, W., Bohling, C., Hohmann, K. & Scheel, D. (2006). Laser-induced plasma spectroscopy for mine detection and verification. *Laser Part. Beams* **24**, 241–247.

Shangguan, H., Casperson, L.W., Shearin, A., Paisley, D. & Prahl, S.A. (1997). Effects of material properties on laser-induced bubble formation in absorbing liquids and on submerged target. *Proc. SPIE* **2869**, 783–791.

Thareja, R.K. & Shukla, S. (2007). Syntheisis and characterization of zinc oxide nanoparticles by laser ablation of zinc in liquid. *Appl. Surf. Scie*. **253**, 8889–8895.

Vogel, A., Schweiger, P., Frieser, A., Asiyo, M.N. & Birngruber, R. (1990). Intraocular Nd:YAG laser surgery: Light-tissue interaction, damage range, and reduction of collateral effects. *IEEE J.QE* **26**, 2240–2260.

Vogel, A., Engelhardt, R., Behnle, U. & Parlitz, U. (1996). Minimisation of cavitation effects in pulsed laser ablation illustrated on laser angioplasty. *Appl. Phys. B* **62**, 173–182.

Vogel, A., Nahen, K., Theisen, D. & Noack, J. (1996). Plasma formation in water by picosecond and nanosecond Nd:YAG laser pulses-Part I: Optical breakdown at threshold and superthreshold irradiance. *IEEE J. Quan. Elecron*. **2**, 847–860.

Venugopalan, V., Guerra III, A., Nahen, K. & Vogel, A. (2002). Role of laser-induced plasma formation in pulsed cellular microsurgery and micromanipulation. *Phys. Rev. Lett.* **88**, 0781031–0781034.

Veiko, V.P., Shakhno, E.A., Smirnov, V.N., Miaskovski, A.M. & Nikishin, G.D. (2006). Laser-induced film deposition by LIFT: Physical mechanisms and applications. *Laser Part. Beams* **24**, 203–209.

Wieger, V., Strassl, M. & Wintner, E. (2006). Pico- and microsecond laser ablation of dental restorative materials. *Laser Part. Beams* **24**, 41–45.

Wolowski, J., Badziak, J., Czarnecka, A., Parys, P., Pisarek, M., Rosinski, M., Turan, R., & Yerci, S. (2007). Application of pulsed laser deposition and laser-induced ion implantation for formation of semiconductor nano-crystallites. *Laser Part. Beams* **25**, 65–69.